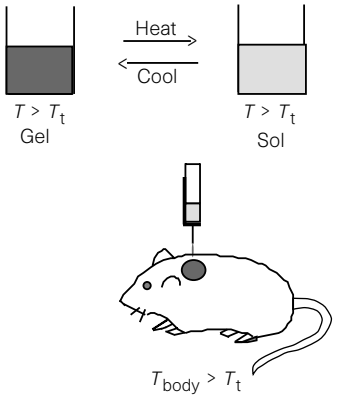

Figure 4 Injectable drug-delivery system. The sol phase containing bioactive agents forms a gel after subcutaneous injection. In the body, it can act as a depot for the controlled release of bioactive agents. T_t is the gel–sol transition temperature.

degradation product of PEO–PLLA–PEO (M_r 5,000–2,040–5,000) triblock copolymer if random scission of PLLA blocks is assumed to be the mechanism of degradation. We note that a 23% aqueous solution of PEO–PLLA–PEO (M_r 5,000–2,040–5,000) becomes a gel at 37 °C. This means one cleavage per triblock copolymer can lead to solubilization of the system.

Based on the thermosensitivity and biodegradability of these polymers, a solvent-free (no organic solvent) injectable system can be designed as a controlled drug carrier. Owing to the sharp phase transition, the sol becomes a gel after subcutaneous injection into the body. As an example, the sol state at 45 °C of PEO–PLLA–PEO (M_r 5,000–2,040–5,000) formed a gel upon subcutaneous injection into a rat (Fig. 4). As a gel in the body, it can act as a sustained-release matrix; this system has several advantages over common drug-delivery systems. First, the formulation is simple and requires no organic solvent. Second, the designed matrix can, if necessary, be stored at or below room temperature as a dry, solid form before administration. Last, there is no requirement for a surgical procedure for implantation. The administration of designed systems can be carried out by simple subcutaneous (or hypodermic-needle) injection after adding warm saline solution (45 °C). The subcutaneous injection of a sol at 45 °C makes causes neither significant pain nor tissue damage[10] because the material is quenched to body temperature in a few seconds. Any pain could be avoided by using a local anaesthetic. The bioactive molecules entrapped in the polymer matrix will be released in the body at first by diffusion, and later by the combination of both diffusion and degradation mechanisms. PEO, PLLA and their degradation products are known to be biocompatible and pharmacologically inactive[11,12], so there is no need for removal of the implant. In contrast, poloxamers are non-biodegradable and enhance plasma cholesterol and triglycerol after intraperitoneal injection in rats[13]. The work that we report here strongly supports the use of copolymer gels for local delivery of bioactive agents, especially protein drugs, with a sustained action. □

Received 3 December 1996; accepted 1 July 1997.

1. Langer, R. New methods of drug delivery. *Science* **249,** 1527–1533 (1990).
2. Ishihara, K., Muramoto, N. & Shinohara, I. Controlled release of organic substances using polymer membrane with responsive function for amino compounds. *J. Appl. Polym. Sci.* **29,** 211–217 (1984).
3. Thomas, J. L., You, H. & Tirrel, D. A. Tuning the response of a pH-sensitive membrane switch. *J. Am. Chem. Soc.* **117,** 2949–2950 (1995).
4. Kwon, I. C., Bae, Y. H. & Kim, S. W. Electrically erodible polymer gel for controlled release of drugs. *Nature* **354,** 291–293 (1991).
5. Bae, Y. H., Okano, T., Hsu, R. & Kim, S. W. Thermo-sensitive polymers as on-off switches for drug release. *Makromol. Chem. Rapid Commun.* **8,** 481–485 (1987).
6. Chen, G. H. & Hoffman, A. S. Graft copolymers that exhibit temperature-induced phase transitions over a wide range of pH. *Nature* **373,** 49–52 (1995).
7. Malstom, M. & Lindman, B. Self-assembly in aqueous block copolymer solutions. *Macromolecules* **25,** 5440–5445 (1992).
8. Youxin, L. & Kissel, T. Synthesis and properties of biodegradable ABA triblock copolymers consisting of poly(L-lactic acid) or poly(L-lactic-co-glycolic acid) A-blocks attached to central poly(oxyethylene) B-blocks. *J. Controlled Release* **27,** 247–257 (1993).
9. Alexandrisdis, P., Holzwarth, J. F. & Hatton, T. A. Micellization of poly(ethylene oxide)-poly(propylene oxide)-poly(ethylene oxide) triblock copolymers in aqueous solution: Thermodynamics of copolymer association. *Macromolecules* **27,** 2414–2425 (1994).
10. Moritz, A. R. & Henrique, F. C. Jr Studies on thermal injury II. The relative importance of time and surface temperature in the causation of cutaneous burns. *Am. J. Pathol.* **23,** 695–720 (1947).
11. Ronneberger, B., Kao, W. J., Anderson, J. A. & Kissel, T. In-vivo biocompatibility study of ABA triblock copolymers consisting of poly(L-lactic-co-glycolic acid) A blocks attached to central poly(oxyethylene) B blocks. *J. Biomed. Mater. Res.* **30,** 31–40 (1996).
12. Zhu, K. J., Lin, X. & Yang, S. Preparation, characterization, and properties of polylactide (PLA)-poly(ethylene glycol) (PEG) copolymers: potential drug carriers. *J. Appl. Polym. Sci.* **39,** 1–9 (1990).
13. Wout, Z. G. M., Pec, E. A., Maggiore, R. H., Palicharla, P. & Johnston, T. Poloxamer 407-mediated changes in plasma cholesterol and triglycerides following intraperitoneal injection to rats. *J. Parenteral Sci. Technol.* **46,** 192–200 (1992).

Acknowledgements. We thank to G. G. Krueger for comments on dermatological issues and J. S. Kim for technical assistance. D. S. Lee was supported by the Ministry of Education of Korea. This work was supported by the University of Utah Research Foundation.

Correspondence and requests for materials should be addressed to S.W.K.

Influence of CO_2 emission rates on the stability of the thermohaline circulation

Thomas F. Stocker & Andreas Schmittner

Climate and Environmental Physics, Physics Institute, University of Bern, Switzerland

Present estimates of the future oceanic uptake of anthropogenic CO_2 and calculations of CO_2-emission scenarios[1] are based on the assumption that the natural carbon cycle is in steady state. But it is well known from palaeoclimate records[2–5] and modelling studies[6–9] that the climate system has more than one equilibrium state, and that perturbations can trigger transitions between them. Anticipated future changes in today's climate system due to human activities have the potential to weaken the thermohaline circulation of the North Atlantic Ocean[10–12], which would greatly modify estimates of future oceanic CO_2 uptake[13]. Here we use a simple coupled atmosphere–ocean climate model to show that the Atlantic thermohaline circulation is not only sensitive to the final atmospheric CO_2 concentration attained, but also depends on the rate of change of the CO_2 concentration in the atmosphere. A modelled increase to 750 parts per million by volume (p.p.m.v.) CO_2 within 100 years (corresponding approximately to a continuation of today's growth rate) leads to a permanent shut-down of the thermohaline circulation. If the final atmospheric concentration of 750 p.p.m.v. CO_2 is attained more slowly, the thermohaline circulation simply slows down. The reason for this rate-sensitive response of the climate system lies with the transfer of buoyancy in the form of heat and fresh water from the uppermost layers of the ocean into the deep waters below. This sensitivity of the simulated thermohaline circulation to the rate of change of atmospheric CO_2 concentration has potentially important implications for the choice of future CO_2-emission scenarios[1].

The burning of fossil fuels, cement production and changes in land use have led to an increase of the atmospheric concentration of CO_2 by almost 30% over the pre-industrial level of 280 p.p.m.v. (ref. 14). Carbon dioxide, and other gases such as CH_4 and N_2O, are the most important greenhouse gases after water vapour and decrease the outgoing longwave radiative flux at the top of the tropopause if their concentrations increase. Recent estimates from several inde-

pendent three-dimensional model simulations suggest that the global mean surface air temperature will increase by 2.1 °C to 4.6 °C for a doubling of atmospheric CO_2 concentrations[1]. Examining an earlier suggestion[15], Manabe and Stouffer[11] showed, using their model, that the Atlantic thermohaline circulation reduces in response to the warming and that a critical threshold value of CO_2 concentration lies between twice and four times the pre-industrial concentration, beyond which the Atlantic thermohaline circulation breaks down. Such permanent changes have a profound impact on the redistribution of heat in the Atlantic region of the Northern Hemisphere, in particular with respect to land–sea temperature contrast. Moreover, a decrease in ventilation and the heating of the sea surface can both reduce the CO_2-uptake of the ocean by as much as about 30% (refs 13, 16) assuming a steady-state natural carbon cycle.

Coupled three-dimensional atmosphere–ocean models are extremely expensive to run which precludes systematic sensitivity studies. In addition, climate drift and the coupling of the different components of these models still pose significant problems especially if future climate states are far from the control climate of these models. Here we use our simplified, three-basin zonally averaged ocean circulation model, coupled to a simple energy-balance model of the atmosphere[17,18]. The model resolves the three ocean basins of the Pacific, Atlantic and Indian oceans which are connected by a circumpolar channel; the ocean dynamics are based on the principle of vorticity balance in a zonally averaged basin[19]. The atmospheric component is a simple energy-balance model[18] which has been supplemented with an active hydrological cycle. This is done by solving the diagnostic equation of the meridional flux of latent heat, **L**, in the zonally averaged atmosphere[20];

$$\nabla\cdot\mathbf{L} = E - P \qquad (1)$$

where $\nabla\cdot$ is the zonally averaged divergence operator in spherical coordinates, and E and P are evaporation and precipitation, respectively. For each latitude, evaporation is calculated as $E = E_1 + E_2 + E_3$ where E_i is the evaporation in ocean basin i depending on basin sea surface temperature and the surface air temperature. The meridional flux of latent heat is taken to be proportional to the meridional moisture gradient, $\mathbf{L} = -K\nabla q$, where K is a constant meridional eddy diffusivity depending on latitude and q is humidity. Following ref. 20 we assume a constant relative humidity, $r = 0.85$, and set $\mathbf{L} = -Kr(\partial q_s/\partial T)\nabla T$, where q_s is the temperature-dependent saturation humidity and T is the surface air temperature. The zonally averaged precipitation P can then be determined from equation (1), but its distribution over the individual ocean basins i requires a closure assumption. Here the ratio P_i/P, where P_i is the precipitation over ocean basin i, is determined from the spin-up of the ocean model by restoring sea surface temperatures and salinities to observed zonal means. In the subsequent experiments, P_i/P is held constant at any latitude. The coupling between the ocean and the atmosphere component of the model involves heat and freshwater fluxes. Wind stress is held constant and associated stabilizing feedbacks[21,22] are neglected here; also the seasonal cycle is not represented. In contrast to most three-dimensional coupled models, no flux correction is applied nor is it necessary to reach a stable steady state. This is important especially if large deviations from the original climate occur[23]. The perturbation due to an increasing concentration of atmospheric CO_2 is incorporated into the energy balance using a constant climate sensitivity parameter[24] (see Fig. 1 legend).

In the present experiments the global mean equilibrium warming for $2 \times CO_2$ is 3.7 °C (exp. 560, Fig. 2) and 7.3 °C for $4 \times CO_2$. We have selected the climate sensitivity $\Delta F_{2\times}$ such that the global mean surface air temperature difference for a CO_2 doubling, $\Delta T_{2\times}$, is consistent with ref. 12. This sensitivity is in the intermediate range of that reported in ref. 1. The increase of the atmospheric CO_2 concentration causes transient changes in our climate model that are very similar to those in three-dimensional coupled atmosphere–ocean models[12,25]. The warmer surface air temperatures increase the saturation vapour pressure and lead to increasing freshwater fluxes in the North Atlantic and to warmer sea surface temperatures. Both

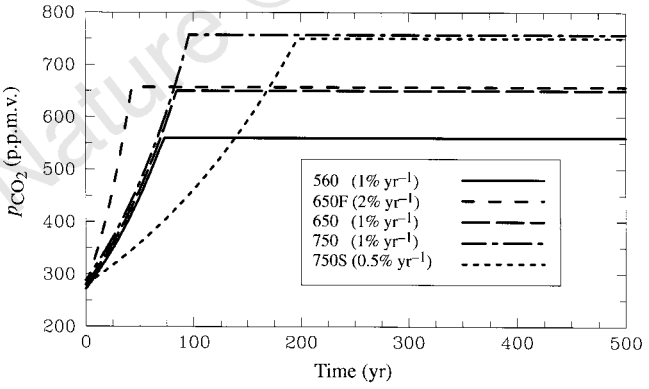

Figure 1 Prescribed evolution of atmospheric CO_2 (equivalent greenhouse gases) for five global warming experiments. The perturbation of the radiative flux in the energy balance model is a function of the CO_2 concentration: $\Delta F(t) = \Delta F_{2\times}\log[p_{CO_2}(t)/280\,\text{p.p.m.v.}]/\log[2]$ according to ref. 24, where $\Delta F(t)$ and $\Delta F_{2\times} = 7.3\,\text{W m}^{-2}$ are the time-dependent and $2 \times CO_2$ energy flux perturbations at the top of the atmosphere, respectively, and $p_{CO_2}(t)$ is the prescribed atmospheric concentration of CO_2 according to the specific scenario. The present scenarios agree with those of ref. 11. The standard rate of CO_2 increase is 1% yr^{-1} compounded (approximately today's value); experiments with a fast rate of 2% yr^{-1} (denoted F) and a slow rate of 0.5% yr^{-1} (denoted S) are also given. The maximum p_{CO_2} values are 560 p.p.m.v. (exp. 560), 650 p.p.m.v. for experiments 650 and 650F, and 750 p.p.m.v. for experiments 750 and 750S. Once the maximum value is reached, $p_{CO_2}(t)$ is held constant. For better visibility, curves are slightly displaced where they would otherwise overlap.

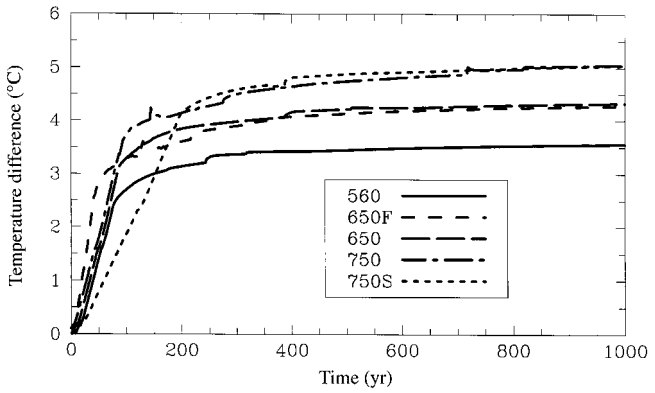

Figure 2 Simulated global mean surface air temperature changes for the five experiments given in Fig. 1. The equilibrium temperature difference is independent of the emission history for a given maximum CO_2 concentration. In these experiments $\Delta F_{2\times} = 7.3\,\text{W m}^{-2}$. Note the considerable delay for final equilibration: it takes >1,000 years to distribute the excess heat in the deep ocean.

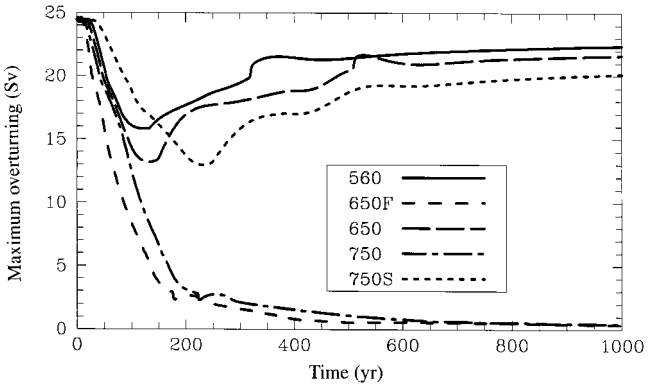

Figure 3 Evolution of the maximum meridional overturning of the North Atlantic in sverdrup (1 Sv = 10^6 m^3 s^{-1}) for the five global warming experiments. In all cases, a reduction is obtained with an amplitude depending on the values of maximum atmospheric CO_2 and on the rate of CO_2 increase. The thermohaline circulation collapses permanently for a maximum concentration of 750 p.p.m.v. with an increase at a rate of 1% yr^{-1} (exp. 750). It recovers, however, and settles to a reduced value if the increase is slower (0.5% yr^{-1}, exp. 750S) or if the final CO_2 level is reduced to 650 p.p.m.v. (exp. 650). Similarly, for a fast increase (exp. 650F) at a rate of 2% yr^{-1} to only 650 p.p.m.v. the circulation collapses. All experiments have been integrated for 10,000 years and no further changes have been observed.

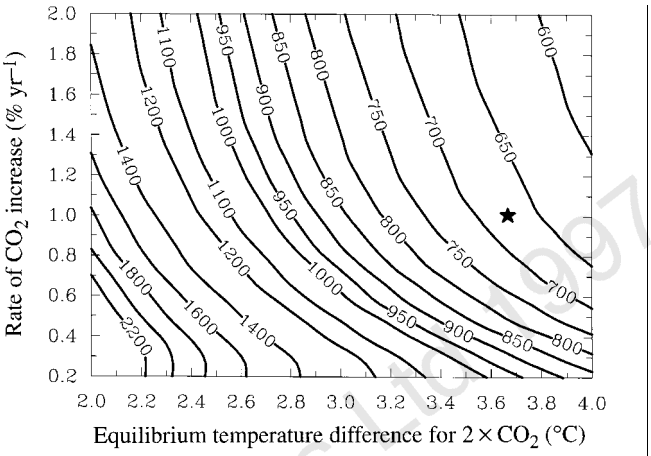

Figure 4 Threshold concentration of atmospheric CO_2 (contours in p.p.m.v.) beyond which the Atlantic thermohaline circulation breaks down permanently as a function of the equilibration surface air temperature difference for a doubling of CO_2, $\Delta T_{2\times}$ (sensitivity of the climate model) and the rate of CO_2 increase in % yr^{-1}. The experiments in Figs 1–3 have been performed for $\Delta T_{2\times} = 3.7$ °C; for a CO_2 increase of 1% yr^{-1} the threshold lies between 650 and 700 p.p.m.v. in this model (denoted by a star). As for any climate model, the actual values depend on model parameters.

processes tend to increase the stratification of the water column and reduce the thermohaline circulation by a maximum of ~34% for a $2 \times CO_2$ experiment (exp. 560, Fig. 3) and a steady-state reduction of ~10%. The sensitivity of the thermohaline circulation in this coupled model is therefore intermediate between that of ref. 25 (10%) and ref. 12 (50%). The timescales of the reduction of the circulation and of its subsequent recovery simulated in exp. 560 (Fig. 3) are in good agreement with those of the same experiment using a three-dimensional, coupled atmosphere–ocean general circulation model[11]. This suggests that, in spite of the simplifications, the present model captures well the main large-scale processes that are relevant for these experiments.

With a CO_2 increase of 1% yr^{-1} (compounded, equivalent greenhouse gases) the thermohaline circulation collapses for maximum CO_2 concentrations of 700 p.p.m.v. and larger. This value depends on the climate sensitivity, $\Delta F_{2\times}$, and various model parameters. The circulation settles into a structurally different equilibrium state which is characterized by the complete absence of deep-water formation in the North Atlantic, much like today's Pacific Ocean. The physical mechanism for this transition is associated with a hysteresis behaviour observed when the Atlantic surface freshwater balance is changed[9,26,27]. Further experiments showed that the increased stratification of the water column due to the warming only, that is, keeping $E - P$ constant in equation (1), is not sufficient to shut down deep water formation. This highlights the important role of changes of the hydrological cycle due to a warmer climate.

We found that in addition to the final CO_2 concentration, the stability of the ocean–atmosphere system is critically dependent on the rate of greenhouse-gas increase. For a slower increase (exp. 750S, Fig. 1) the Atlantic thermohaline circulation first reduces but then recovers, at a circulation weakened by ~15% (Fig. 3). Deep water is still being formed in the North Atlantic after CO_2 has reached its maximum value. As long as the Atlantic thermohaline circulation is not shut down, excess heat and fresh water, which tend to reduce the circulation, are still efficiently redistributed by advection, diffusion and especially convection. Therefore, the critical reduction of surface density, beyond which deep-water formation is inhibited, is not reached in this case. A slower warming thus tends to stabilize the system. But once the deep-water formation breaks down owing to a faster increase of atmospheric CO_2 and air temperature (Fig. 2), the subsequent process is self-sustaining: the absence of convection in the North Atlantic leads to an increased load of heat and fresh water in the upper layers of the ocean with a corresponding stronger stratification. A similar effect of the dependence of the stability of thermohaline circulation on the rate of perturbation changes was found in ocean-only models subject to localized freshwater injections[26,28].

There is still considerable uncertainty about the climate sensitivity of current climate models. We therefore investigated the threshold atmospheric CO_2 concentration beyond which formation of North Atlantic Deep Water is inhibited as a function of the equilibration temperature change for $2 \times CO_2$, $\Delta T_{2\times}$ and the rate of change of CO_2 in % yr^{-1} (Fig. 4). This is the result of an extensive sensitivity study that is possible with this coupled climate model. For a given rate $\partial \Delta F/\partial t$ we made 1,000-yr experiments for increasing values of ΔF, the change in the radiation balance at the final CO_2 concentration, and determined the threshold value at which the thermohaline circulation shuts down permanently. For easier reference we then plot this result as contour lines of the threshold CO_2 concentration in a diagram where $p_{CO_2}^{-1}(\partial p_{CO_2}/\partial t)$ is plotted against $\Delta T_{2\times}$ (Fig. 4). For a typical climate sensitivity of $\Delta T_{2\times} = 3.7$ °C and the present increase of CO_2 at 1% yr^{-1}, the model yields a critical level of just below 700 p.p.m.v. For rates below the present value of 1% yr^{-1}, the critical level is increasingly sensitive to the rate of CO_2 increase. A reduction of the rate of warming increases the critical level considerably. It is desirable to construct such a diagram with state-of-the-art three-dimensional coupled atmosphere–ocean models which contain more feedback processes and better spatial resolution than the present model. Furthermore, the implications of even a partial reduction of the Atlantic thermohaline circulation for biogeochemical cycles need to be investigated in greater detail.

The present results confirm an earlier study[11] which concluded that the atmosphere–ocean system contains critical levels of atmospheric CO_2 beyond which irreversible changes of the Atlantic thermohaline circulation are likely. Such changes would have also important direct and indirect consequences for the distribution of antropogenic carbon: a strong reduction of ventilation decreases the transport of excess carbon and heat into the deep ocean. The latter leads to an enhanced warming of the upper layers of the ocean which, in turn, decreases the solubility of CO_2 and results in a further increase of atmospheric CO_2. This feedback mechanism has the tendency to further destabilize the thermohaline circulation.

Our finding, that these critical levels also depend on the rate of CO_2 increase, is also relevant for decisions about the choice of a particular scenario of future greenhouse gas emissions. In the future, such decisions will not only need to consider the stabilization concentration or the economic cost of emission reduction to reach this concentration[29], but also take into account critical limits on the rate of greenhouse gas increase of the atmosphere. □

Received 21 April; accepted 30 June 1997.

1. Houghton, J. T. *et al.* (eds) *Climate Change 1995: The Science of Climate Change* (Cambridge Univ. Press, 1996).
2. Oeschger, H. *et al.* in *Climate Processes and Climate Sensitivity* (eds Hansen, J. E. & Takahashi, T.) 299–306 (Geophys. Monogr. 29, Am. Geophys. Un., Washington DC, 1984).
3. Broecker, W. S., Peteet, D. & Rind, D. Does the ocean–atmosphere system have more than one stable mode of operation? *Nature* **315,** 21–25 (1985).
4. Broecker, W. S. & Denton, G. H. The role of ocean-atmosphere reorganizations in glacial cycles. *Geochim. Cosmochim. Acta* **53,** 2465–2501 (1989).
5. Bond, G. *et al.* Correlations between climate records from North Atlantic sediments and Greenland ice. *Nature* **365,** 143–147 (1993).
6. Bryan, F. High-latitude salinity effects and interhemispheric thermohaline circulations. *Nature* **323,** 301–304 (1986).
7. Manabe, S. & Stouffer, R. J. Two stable equilibria of a coupled ocean-atmosphere model. *J. Clim.* **1,** 841–866 (1988).
8. Maier-Reimer, E. & Mikolajewicz, U. *Experiments with an OGCM on the cause of the Younger Dryas* 1–13 (Tech. Rep. 39, Max-Planck-Inst. für Meteorol., Hamburg, 1989).
9. Stocker, T. F. & Wright, D. G. Rapid transitions of the ocean's deep circulation induced by changes in surface water fluxes. *Nature* **351,** 729–732 (1991).
10. Manabe, S., Stouffer, R. J., Spelman, M. J. & Bryan, K. Transient responses of a coupled ocean-atmosphere model to gradual changes of atmospheric CO_2. Part I: Annual mean response. *J. Clim.* **4,** 785–818 (1991).
11. Manabe, S. & Stouffer, R. J. Century-scale effects of increased atmospheric CO_2 on the ocean–atmosphere system. *Nature* **364,** 215–218 (1993).
12. Manabe, S. & Stouffer, R. J. Multiple-century response of a coupled ocean-atmosphere model to an increase of atmospheric carbon dioxide. *J. Clim.* **7,** 5–23 (1994).
13. Sarmiento, J. L. & Le Queré, C. Oceanic carbon dioxide in a model of century-scale global warming. *Science* **274,** 1346–1350 (1996).
14. Neftel, A., Oeschger, H., Staffelbach, T. & Stauffer, B. CO_2 record in the Byrd ice core 50,000–5,000 years BP. *Nature* **331,** 609–611 (1988).
15. Broecker, W. S. Unpleasant surprises in the greenhouse? *Nature* **328,** 123–126 (1987).
16. Maier-Reimer, E., Mikolajewicz, U. & Winguth, A. Future ocean uptake of CO_2: interaction between ocean circulation and biology. *Clim. Dyn.* **12,** 711–721 (1996).
17. Wright, D. G. & Stocker, T. F. Sensitivities of a zonally averaged global ocean circulation model. *J. Geophys. Res.* **97,** 12707–12730 (1992).
18. Stocker, T. F., Wright, D. G. & Mysak, L. A. A zonally averaged, coupled ocean-atmosphere model for paleoclimate studies. *J. Clim.* **5,** 773–797 (1992).
19. Wright, D. G., Vreugdenhil, C. B. & Hughes, T. M. Vorticity dynamics and zonally averaged ocean circulation models. *J. Phys. Oceanogr.* **25,** 2141–2154 (1995).
20. Chen, D., Gerdes, R. & Lohmann, G. A 1-D atmospheric energy balance model developed for ocean modelling. *Theor. Appl. Climatol.* **51,** 25–38 (1995).
21. Weaver, A. J., Marotzke, J., Cummins, P. F. & Sarachik, E. S. Stability and variability of the thermohaline circulation. *J. Phys. Oceanogr.* **23,** 39–60 (1993).
22. Schiller, A., Mikolajewicz, U. & Voss, R. The stability of the thermohaline circulation in a coupled ocean-atmosphere general circulation model. *Clim. Dyn.* **13,** 325–347 (1997).
23. Egger, J. Flux correction: tests with a simple ocean-atmosphere model. *Clim. Dyn.* **13,** 285–292 (1997).
24. Shine, K. P., Derwent, R. G., Wuebbles, D. J. & Morcrette, J.-J. in *Climate Change: The IPCC Scientific Assessment* (eds Houghton, J. Y., Jenkins, G. J. & Ephraums, J. J.) 41–68 (Cambridge Univ. Press, 1990).
25. Johns, T. C. *et al.* The second Hadley Centre coupled ocean-atmosphere GCM: model description, spinup and validation. *Clim. Dyn.* **13,** 103–134 (1997).
26. Mikolajewicz, U. & Maier-Reimer, E. Mixed boundary conditions in ocean general circulation models and their influence on the stability of the model's conveyor belt. *J. Geophys. Res.* **99,** 22633–22644 (1994).
27. Rahmstorf, S. Bifurcations of the Atlantic thermohaline circulation in response to changes in the hydrological cycle. *Nature* **378,** 145–149 (1995).
28. Rahmstorf, S., Marotzke, J. & Willebrand, J. in *The Warmwatersphere of the North Atlantic Ocean* (ed. Krauss, W.) 129–157 (Bornträger, Berlin, 1996).
29. Wigley, T. M. L., Richels, R. & Edmonds, J. A. Economic and environmental choices in the stabilization of atmospheric CO_2 concentrations. *Nature* **379,** 240–243 (1996).

Acknowledgements. We thank N. Gruber, F. Joos, O. Marchal, H. Oeschger, S. Rahmstorf, A. Weaver and D. Wright for comments. This work was supported by the Swiss National Science Foundation.

Correspondence should be addressed to T.F.S. (e-mail: stocker@climate.unibe.ch).

Critical behaviour and the evolution of fault strength during earthquake cycles

Moritz Heimpel

Institut für Geophysik, Universität Göttingen, D-37075 Göttingen, Germany

The problem of how fault rheology and heterogeneity interact to produce the observed scaling of earthquakes (such as the power-law moment–frequency relationship) remains largely unsolved. Rock friction experiments have elucidated the properties of smooth faults[1–3], but seem insufficient to explain the observed complexity of real fault dynamics[4,5]. The recognition of a connection between fault-related processes and critical phenomena in other physical systems, together with numerical models of repeated earthquakes, have resulted in significant progress in the theoretical interpretation of earthquake scaling[4–14]. But fault rheology and heterogeneity have so far been treated separately. Here I attempt to unify the requirements of fault rheology and heterogeneity using numerical calculations of quantized slip in an elastic continuum. I show that cyclical fault strength evolves naturally by means of a statistical selection for high-strength fault patches (asperities), resulting in the accumulation and eventual failure of those asperities. The applicability of these results to real fault systems is supported by a recent analysis of time-dependent earthquake statistics[15]. These results imply that self-similarity and criticality on a fault emerge during an earthquake cycle, and suggest that the character of local seismicity can be useful in earthquake forecasting by revealing how advanced a fault is within its cycle.

During an earthquake the state of the fault–crust system changes rapidly. Stress is released and the fault strength drops. Between earthquakes, fault stress and strength recover through slip- and time-dependent healing. The physics of this cyclical process can be understood in terms of the evolution of a population of isolated contact surfaces[16–18]. Such a population arises when two rough fault surfaces are pressed together with insufficient normal force to close apertures. An important parameter controlling this evolution is the minimum critical slip L_{min} required to change the strength of a population of contacts. Although fault surfaces are fractal and self-affine[19–21], it has been shown that two unmatched surfaces pressed together produce a maximum distance λ_c between contact surfaces (ref. 16), implying a minimum critical slip distance $L_{min} \approx \lambda_c$. Estimates of λ_c (and thus L_{min}) for natural fault surfaces typically range from 10^{-3} to 10^{-2} m (refs 16–18). For natural faults the presence of gouge also affects the scaling of L_{min}; although not explicitly treated here, its effect is analogous to increasing fault surface roughness[22].

In the numerical model presented here, λ_c (and thus also L_{min}) is further interpreted to represent the minimum slip required to statistically decorrelate the local yield strength on a fault patch. This is clearly applicable if fault heterogeneity results from a diversity of loading and geometrical conditions on the scale of individual contacts. The model uses exact solutions for quantized slip on a fault surface embedded in a three-dimensional elastic medium. The model may be classified as inherently discrete (as defined in ref. 4) because, as discussed below, the yield strength of individual model cells can change abruptly. The main assumptions are as follows. (1) Inertia is neglected (quasi-static approximation). (2) Background stress increases uniformly over the fault plane. Time steps are chosen so that a quake initiates at a single numerical cell at every time step. (3) Slip is quantized; each of the $\sim 10^8$ discrete slips